
Using finite element modelling and simulations to test MotoGP race bikes

Terje Rølvåg

Department of Engineering Design and Materials,
NTNU,
Richard Birkelands veg 2B, N-7491 Trondheim, Norway
Email: terje.rolvag@ntnu.no

Abstract: The primary objective of this study is the development of a robust numerical simulation model that captures the dynamical characteristics of the Ilmor X³ 2007 MotoGP racing bike. This model can be reconfigured to vary the weight distribution, the stiffness and the damping properties that affect wheelies and stoppies. The model includes tyre models, the driveline from the engine to the rear wheel and a steering system to control the bike in ride simulations. Sensitivity simulations are performed to study the effect of different bike configurations on wheelies and stoppies, i.e., the front and rear wheel lifts that occur during maximum acceleration and braking of the bike. Various modifications are made to the FE-based simulation model to investigate the effect of these changes on the ride behaviour.

Keywords: racing bikes; finite element analysis; system dynamics; control systems; MotoGP.

Reference to this paper should be made as follows: Rølvåg, T. (2015) 'Using finite element modelling and simulations to test MotoGP race bikes', *Int. J. Vehicle Systems Modelling and Testing*, Vol. 10, No. 1, pp.74–106.

Biographical notes: Terje Rølvåg holds an MSc and a PhD within finite element dynamics of elastic mechanisms and control from NTH. His publications are mainly within non-linear finite element dynamics and active damping of elastic mechanisms. He has been central in developing FEDEM, a finite element-based modelling and simulation tool with multidisciplinary capabilities (see www.fedem.com). He has also established several engineering companies and optimised products for the automotive, offshore and aerospace industries. His research interests cover computer science applied for engineering applications focusing on simulation of behaviour and strength of electromechanical products.

1 Introduction

MotoGP bikes are the most advanced racing bikes, and the solutions launched by the development teams for these bikes are implemented in public racing bikes within a few years. The use of lightweight materials, such as aluminium, titanium, magnesium and carbon fibre-reinforced plastics, along with highly sophisticated suspension and brake units and extreme engine packages, make MotoGP bikes the most advanced and fastest track bikes in the world. Producing a high-performance MotoGP motorcycle prototype

entails extensive engineering before skilled riders can evaluate the performance and handling qualities of the physical system. Unfortunately, the brief period between hectic MotoGP racing seasons limits the number of physical tests that can be performed during the design process. Thus, virtual prototyping can play an important role in this process, as mentioned in Cossalter and Lot (2002), Evangelou et al. (2006), Frezza and Beghi (2003), Hauser and Saccon (2006), Sharp and Limebeer (2001) and Sharp et al. (2004).

2 Background

Eskil Suter, a former Grand Prix motorcycle road racer from Switzerland, who is currently a motorcycle chassis designer, founded a company named Suter Racing Technology (SRT) in 1996. In 2006 and 2007, SRT collaborated with Ilmor Engineering on the chassis design of the 800 cc Ilmor X³ motorcycle (Crash Media Group, 2006). Unfortunately, this collaboration was terminated for financial reasons in late 2007, which has limited access to physical test data that could validate the simulation results presented in this paper. However, the inputs to the model developed in this paper were based on component tests and data received from SRT. Observations and test drives by SRT drivers later confirmed the sensitivity results from the simulations.

This study was initiated by a request from SRT. The SRT MotoGP engineering team needed to conduct virtual tests of their motorcycle to analyse its performance and assess design trade-offs.

State-of-the-art motorcycle models, such as those described in Cossalter and Lot (2002) and Sharp and Limebeer (2001), consist of interconnected rigid bodies with a suspension and other flexible components that are supplemented by sophisticated tyre and engine models (Pacejka, 2002; Pacejka and Bakker, 1991). SRT has tested commercial codes based on rigid body formulations without success. These codes performed well numerically; however, the codes could not be used to simulate wheelies and stoppies because of singularity problems and unstable numerical performance.

SRT also wanted to perform stress and modal analyses to optimise the structural composite frame stiffness to mass ratio. Therefore, the primary question in this research study was whether non-linear finite element programmes, such as those given in Fedem Technology (2013) and LMS (2014), could be used to model and simulate motorcycle ride and handling. The commercial Fedem software was selected because it includes embedded support of control system modelling (Fedem Technology, 2013). Structural optimisation was performed but is not presented in this paper.

3 The Fedem modelling approach

Fedem is a multidisciplinary simulation scheme that is based on a non-linear finite element scheme and control system modelling and simulation. In Fedem, structural components are represented by FE models (superelements). The superelement mass and stiffness matrices are reduced using static or component mode synthesis (CMS) reduction (Sivertsen, 2001). Each superelement is imported, positioned and used as a link in the Fedem bike assembly. A co-rotated frame is associated with each link (superelement), and the elastic displacements and stress results are calculated relative to this frame. Large rotations and displacements of the links are included in the model, but the elastic

displacements of each link are assumed to be small. The links are connected together with various joint types (revolute, ball, cam, etc.). All of the joint types are based on master and slave techniques that have been shown to be more numerically robust than using Lagrange multipliers when the model size (i.e., the degrees of freedom) increases. Lumped masses and inertias may be applied directly to the motorcycle model. The basic FE formulation and the applied model reduction preserve the mass distribution and gyroscopic effects. Non-linear vehicle loads, front and rear dampers and springs can be attached between nodes to the structural parts. The control system is created in a 2D environment and coupled together with the 3D motorcycle model (which is both embedded in Fedem). The solvers are based on various numerical methods, such as Newton-Raphson and Newmark integration schemes, and all of the structural and control system variables are solved for simultaneously using an iterative method. The stresses can be solved at specified mechanism configurations/time steps. A major advantage of the finite element approach is that problems related to over-constrained (rigid body) parts are eliminated. Rigid bodies have a maximum of 6 degrees of freedom, which sometimes limit the joint modelling capabilities and the load transfer between structural vehicle components.

These integrated Fedem capabilities support a multidisciplinary modelling and simulation environment that enables racing bike designers to perform virtual tests and optimisation. Even when structural deflection is of minor importance, the robust performance and accuracy of Fedem justify the extra degrees of freedom introduced by the FE approach.

4 Fedem simulation approach

It is essential to consider the geometry and structural properties of the racing bike links in a dynamic simulation of a flexible body. However, a simplified geometry is often used in the initial dynamic simulation, as in the feasibility studies of a proposed bike design, for instance. In this study, the flexible body dynamics are initially not essential; thus, simplified geometries should produce an acceptable correspondence to the performance of the real Ilmor bike.

The primary benefit obtained from using the finite element method is its robust numerical performance and the elimination of over-constrained rigid bodies because of joint modelling requirements. The various joint types are modelled using a master and slave node technique that eliminates artificial stiffness (Sivertsen, 2001). The finite element formulation does not limit the number of joint constraints to 6, but supports realistic connections between the structural motorcycle components. This feature is important for enabling correct load transfer between the structural components that affect ride and handling.

In Fedem, the CMS model reduction eliminates all of the nodes that are not used as connection points in the motorcycle assembly. The remaining external supernode displacements for each superelement (i.e., the structural FE component) are stored in a system displacement vector r . The non-linear dynamical equation of motion of the bike at

the time step k can then be written in an incremental (linearised) form as follows (Fedem Technology, 2013):

$${}^i M_k {}^i \ddot{\Delta}_k + {}^i C_k {}^i \dot{\Delta}_k + {}^i K_k {}^i \Delta_k = {}^i Q_{k+1} - [{}^{i-1} F_{k+1}^I + {}^{i-1} F_{k+1}^D + {}^{i-1} F_{k+1}^S],$$

where the index i indicates the iteration number. The maximum number of iterations was set to 50 because of the high-speed non-linear dynamics of the motorbike. The system matrices M_k , C_k and K_k were only updated for the first 50 iterations (which were modified Newton-Raphson iterations). The minimum number of iterations was set to 2 to balance the mechanical and control system forces. With a time step of 0.001s, the required number of iterations varied between 2 and 7 for a typical 0 to 100 km/h acceleration sequence.

The system mass matrix M_k is CMS-reduced and therefore is always fully populated even if a lumped mass representation is used for the selected finite elements. Therefore, the gyro effects that have a major impact on the racing bike dynamics are correctly represented. The reduced system damping matrix C_k is proportional to the mass and the stiffness (Rayleigh damping) (Sivertsen, 2001). The linear and non-linear lumped masses/inertias, dampers and springs representing the racing bike components that are not modelled by the FEMs are directly added to the system matrices.

5 Ilmor X³ modelling

A wide range of physical properties must be estimated and implemented during the X³ modelling process. The model formulation enables different configurations of the bike suspension, the weight distribution and the component geometry to be tested. Virtual testing provides almost unlimited possibilities of capturing measurements of all types of movements, velocities, forces and gyroscopic effects that act on the bike and between its different components. Many of these values are difficult to measure for a real bike and are sometimes impossible to obtain between or during the racing seasons. The primary purpose of the X³ modelling and simulations is therefore to investigate the trends (sensitivities) associated with varying the different physical properties and configurations of the virtual model.

5.1 Modelling requirements

The Ilmor X³ MotoGP bike is a very complicated system of high-performance mechanical and electrical components. The model was simplified to formulate a representative and computationally efficient X³ model. To reduce the complexity of the model and the simulation and still obtain reliable simulation results, the author had to obtain a considerable amount of information from the design and test engineers/riders. This process was challenging because of both technical and driver issues, which are detailed below.

- engineers need to understand how a MotoGP bike is handled by drivers (in terms of steering, braking, etc.)
- engineers from different disciplines are located in different areas (ref. UK, Norway and Switzerland)
- engineers and test drivers use inconsistent terminology
- there is an absence of test data on components and tyres.

An overview of the X³ model requirements and a comprehensive description of the overall X³ architecture are given in Giussani (2007) and Weiby (2007).

Figure 1 Ilmor X³ model requirements (see online version for colours)

Requirements for the Fedem model:	Must:	Should:
Correct geometry	√	
Correct weight distribution (adjustable)	√	
Suspension properties which correspond to the real suspension units		√
Adjustable spring stiffness	√	
Adjustable damper coefficients	√	
Include tyre models	√	
Possibility of studying vibrations in chassis		√
Adjustable wheelbase		√
Adjustable pivot axle		√
Include gyroscopic effects	√	
Driveline with gear ratios	√	
Steering system for performing manoeuvres	√	
Engine control system		√

5.2 Modelling process

The bike modelling was performed in Catia, whereas the meshing and material properties were added in NX. The FE models were transferred to, assembled and simulated in Fedem. The weight and centre of gravity (CG) in the simulation model corresponded to that of the Ilmor X³ MotoGP 2007 racing bike. The model included advanced suspension units that were represented by non-linear springs and dampers that are added to the Fedem model.

Tyre models based on Pacejka and Bakker (1991) were used to account for the flexibility and slip of real tyres. The weight distribution, stiffness and damping, together with many other model parameters, can be modified. In this paper, only the tyre properties for the ride simulations are important because handling (manoeuvring) was not tested. The rider position was modelled as being fixed for the same reason. In handling simulations, the rider significantly affects the bike behaviour, but during wheelies and stoppies, the rider position can be assumed as fixed (Giussani, 2007).

The primary rotating components in the engine were included, and the use of gear connections ensured that these transmission components had the same speed and properties as the real bike. The engine performance of the model was based on test results for the Ilmor engine. This engine performance and other forces, such as the air drag and steering forces, were regulated by a control system that was fully embedded in the FE model. This sophisticated control system calculated steering signals to maintain the balance of the bike and make it manoeuvrable.

The most demanding task was to understand and implement counter-steering in the simulation model. The Ilmor X³ bike is shown in Figure 2.

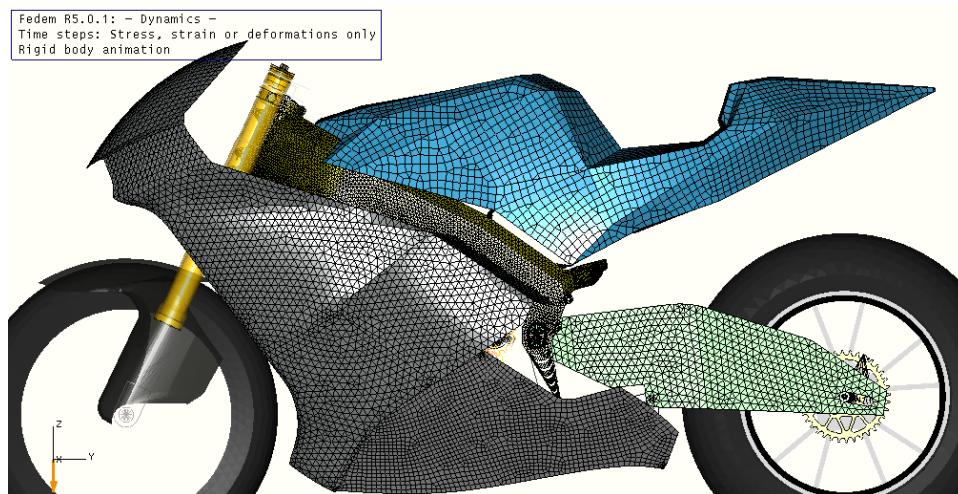
Figure 2 Ilmor X³ MotoGP racing bike (see online version for colours)



5.3 Ilmor X³ structural FE models (links)

To import the modelled parts into Fedem for use as mechanism links, these parts had to be idealised and meshed in NX. The mesh was optimised for the dynamic simulations but not for the detailed stress analysis. Figure 3 shows simplified representations of some of the FE models of the body. These models consisted of shell elements with 3 and 4 nodes. The engine, crankshaft, clutch and gearbox were modelled using solid tetrahedral 10-node elements. The material data were modelled as prescribed by SRT.

Figure 3 FEM Ilmor X³ assembly (see online version for colours)



In a fully FE-based dynamic solver such as Fedem, the static system matrices represent both the rigid body displacements and the dominant elastic displacements. In Fedem, the retained (super) nodes used as connection points were identified as triads with local

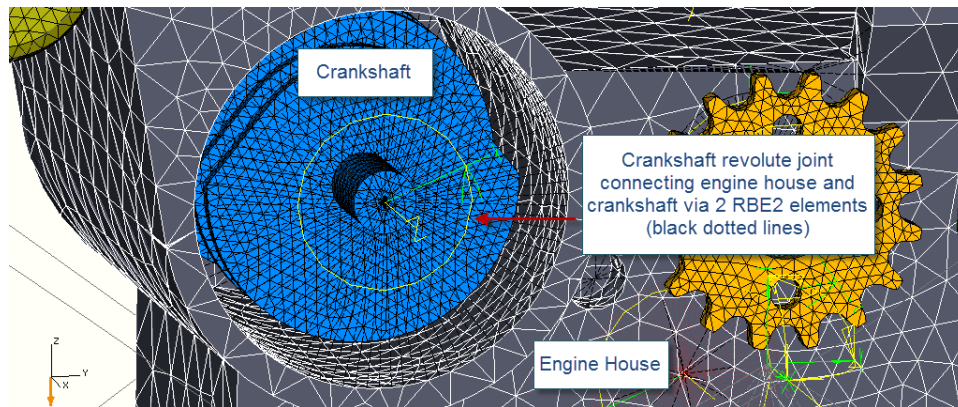
coordinate systems. These coordinate systems were used to align the dampers, springs and joint directions of the Ilmor model. The fixed interface normal modes simply augmented the internal displacements used in the stress analysis. These modes had no effect on the simulated Ilmor handling performance.

5.4 *Ilmor X³ joint modelling*

To prepare the links for simulation in Fedem, it was necessary to determine where the different links should be connected by joints. A Fedem joint connected at least one master and one slave node (triad) from two links to facilitate constrained 3D translational or rotational motion between the links. The master or slave node could be attached to other nodes on the same link via RBE2 or RBE3 elements to improve the structural load distribution.

Figure 4 illustrates how one of two revolute joints (shown in yellow) enable rotational motion between the Ilmor engine block and the crank shaft. In this study, both rotating and counter-rotating crankshafts were tested to reduce the wheelie effect.

Figure 4 Ilmor X³ joint modelling (see online version for colours)



This master and slave-based joint modelling technique is very robust, and the reduced FE models eliminated the traditional problems that are encountered with over-constrained rigid bodies. In the example given above, the crankshafts were constrained using two revolute joints (only one joint is shown), thereby imposing ten constrained DOFs. The constraints on the two physical crankshaft bearings are designed to produce the correct constrained bearing forces. A rigid body formulation can only represent one revolute joint, whereas two joints impose ten constraints on one rigid body part with six DOFs.

5.5 *Ilmor X³ assembly FE model*

The refined geometry of the final model matched the dimensions of the Ilmor X³. The suspension properties of the model were tuned using the measurements of the real bike (LMS, 2014). The tyre models matched the new tyres that are used in the MotoGP. The

dimensions and the radial stiffness were correct, and the tyre models could tolerate large camber angles.

Figure 5 Final Ilmor X³ model (see online version for colours)

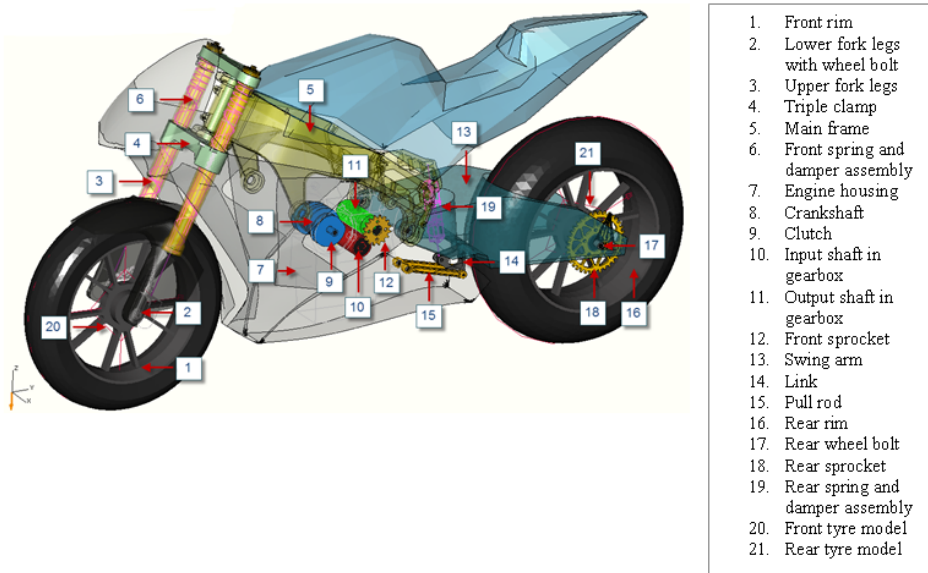


Figure 5 shows the Ilmor model with transparent fairing to display the engine components and more of the modelled geometry. Some components are shown as lines to visualise the suspension units and the tyre models. The gear connections and loads are not shown.

5.6 Suspension modelling

The coefficients of the springs and dampers in the simulation model were determined to match those of the real bike suspension. The fork assembly is quite complicated and consists of several structures and gas and oil-based springs and dampers. The model captured the essential properties of the spring and damper in the fork as well as the overall length and end effects that limit the maximum stroke lengths. This motorcycle is fitted with an upside down telescopic front fork suspension system and a swing-arm-based rear suspension that incorporates a single spring-damper unit linked mechanically to the swing-arm, a so-called monoshock suspension. These two suspension units are further described in the following sections.

5.7 Front suspension modelling

The front suspension is produced by Öhlins and is an upside down type of fork, i.e., the internal tube is in the lower position and is fixed to the wheel. This type of fork has been used in racing since the early nineties. These fork legs are illustrated in Figure 6.

Figure 6 Öhlins racing bike fork (see online version for colours)

To simulate the fork suspension unit realistically, all of the properties of the fork had to be identified and incorporated into the simulation model. The primary spring (number 2 in Figure 9) in each of the fork legs had a stiffness of 9,000 [N/m] and a preload of 0.045 [m]. The preload did not alter the spring stiffness but simulated the effect of a stiffer spring. The preload was used to adjust how much travel resulted from placing a control unit under a certain load.

The top out spring that worked against the extension of the fork had a stiffness of 3,500 [N/m] and a length of 0.04 [m]. These top out springs only affected the first 0.04 m of the stroke (which was measured relative to the full extension of the spring). The maximum travel distance of the fork was 0.13 m. These properties were implemented using the non-linear function shown in Figure 7. This spring function was used for a free joint between the upper and lower fork. The same method was used to model the rear suspension.

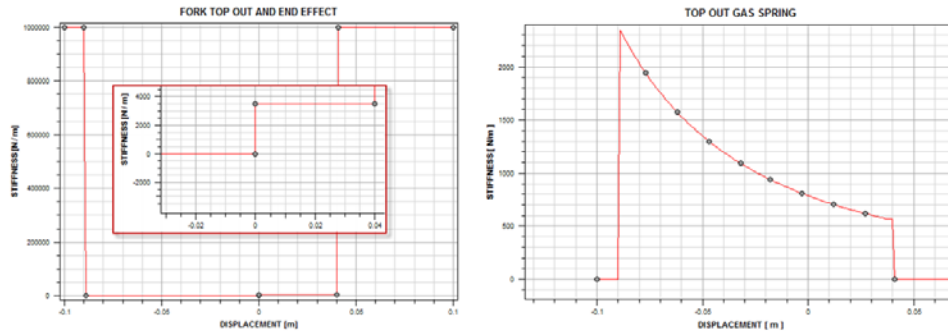
During the compression phase, the volume of air contained in the fork diminishes, which serves a double function.

- 1 The air acts as another spring that is characterised by a high progressive rate.
- 2 Pressure is created inside the fork, which prevents cavitation problems and foam from forming on the oil-to-air contact surface (Cheney Engineering, 2007).

The effect of a progressive air spring (number 1 in Figure 9) was incorporated into the model using a function (see Figure 7) that was used to describe the behaviour of a spring in each of the fork legs. This function included the properties of the gas pressure inside the fork, which depended on the front wheel stroke. This gas pressure created a force that acted to extend the fork; however, the force was zero when the fork reached full extension. This force created by the gas pressure was expressed as a function of the stroke length in Fedem Technology (2013). Cavitation corresponds to the creation of gas bubbles in the oil near the bleed orifices in the damper piston at a high damper velocity (i.e., above the optimum working velocity). Cavitation is caused by a large pressure difference on each side of the orifice. These effects are neglected in the Fedem model because a suitably configured fork ensures that cavitation occurs rarely. Advanced dampers maintain the oil under a sufficiently high pressure that gas is unlikely to form. Real dampers can be tested in a so-called 'shock dyno'. These apparatuses can be used to

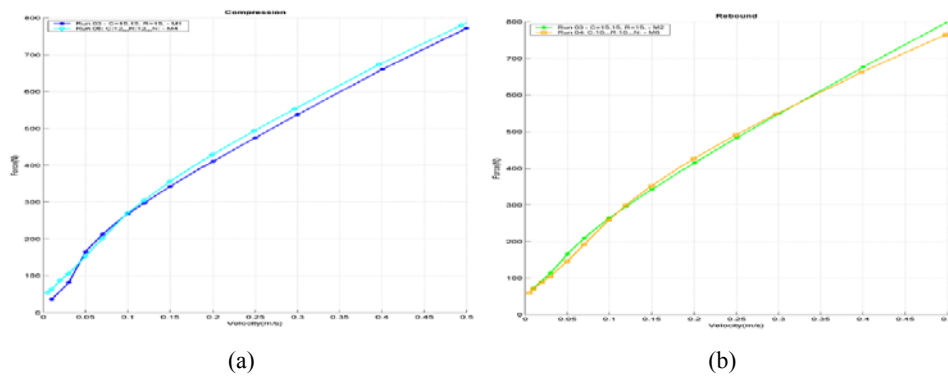
test dampers over a wide range of velocities, measure the damping force and determine whether cavitation has occurred.

Figure 7 Top out fork and gas spring (see online version for colours)



The damper properties in each fork leg were formulated and implemented using graphs that were measured by Öhlins (Figure 8).

Figure 8 Measured and implemented Öhlins damper forces vs. velocity in, (a) compression (b) rebound (see online version for colours)

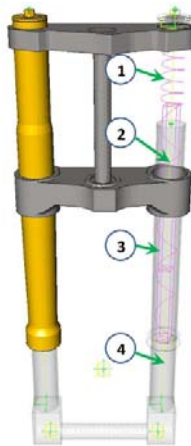


The static load on the front wheel was approximately 1,142 N for a fork angle of 24.5°, which corresponded to a load of 1,039 N in the direction of the fork. Using the fork properties given by SRT, this load resulted in an initial fork compression of approximately 40 mm, which was measured relative to the fully extended length of the fork.

The sliding fork motion between the lower and upper fork legs was implemented by two prismatic joints that allowed translational motion while preserving the correct fork leg bending stiffness (i.e., these joints were flexible and based on master and slave nodes). The suspension properties of each fork leg were modelled by two springs and a free joint that acted as a spring, and a damper. The spring on top of the model (number 1 in Figure 9) simulated the gas inside the fork. When the fork was fully extended, the gas pressure inside the fork was 0.1013 MPa, which was equal to the air pressure outside the fork: therefore, the gas had no effect. During the fork compression, the gas pressure rose

and behaved as a progressive spring (see Figure 7). The largest fork spring (number 2 in Figure 9) was the primary spring and had a stiffness of 9 N/mm. The damper (number 3 in Figure 9) was non-linear and had a different damper coefficient in compression and rebound (see Figure 8). The free joint acted as a spring and performed the same function as the top out spring in the fork (number 4 in Figure 9). This spring only worked during the fork extension, and this free joint also included very stiff springs that acted as ‘bump stops’ to ensure that the wheel stroke never exceeded 130 mm. The fork could be extended to 40 mm and compressed to 90 mm from its equilibrium position. All of the springs (and the damper) were coupled in parallel in each fork leg because they were not directly connected to each other but between the same components.

Figure 9 Fork suspension model (see online version for colours)



The detailed properties and tuning of the fork springs and dampers can be found in Giussani (2007) and Weiby (2007). Comparing the fork response data as a function of the front wheel stroke showed that the modelled fork had the same spring stiffness as the real fork. The dampers also had approximately the same coefficients as the real dampers (i.e., a 6% maximum deviation over the measured range). Minor errors in the damper characteristics could have resulted from manual reading of the graphs of the damper force versus the velocity.

The rake angle (i.e., the fork angle) may be adjusted both for the real bike and the model: however, for a typical bike configuration, the rake angle is approximately 24.5° from the vertical. A smaller rake angle (a steeper fork) usually results in a more agile bike but makes the bike more unstable because of the trail reduction. The rake angle in the model was set to 24.5° .

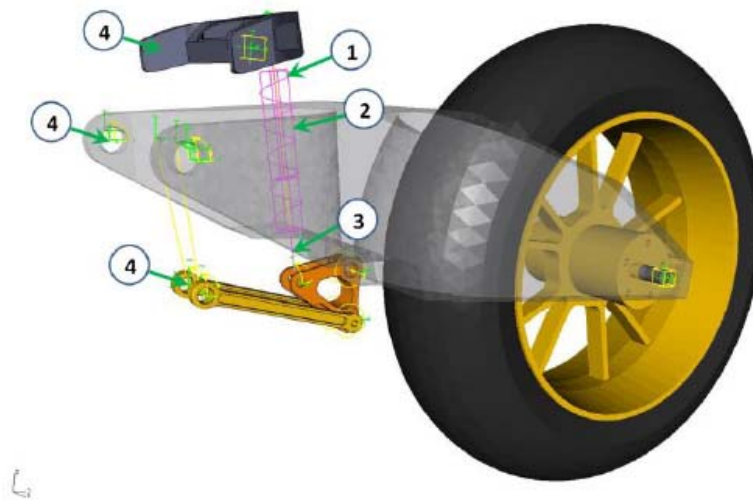
5.8 Rear suspension modelling

There are effectively three chassis phases during cornering: a nose-down entry, steady cornering and a nose-up exit. The behaviour of the bike in these different phases and in a straight line can provide a good indication of how the suspension configuration is functioning. These types of manoeuvres can be performed using the simulation model, which supports virtual suspension testing and optimisation. In the virtual model, any

value can be measured at any time step. This project was initially limited to study the final phase: the nose-up exit. Generally, this phase corresponds to the acceleration of the bike out of corners. The other phases during cornering were also briefly studied.

The rear suspension contains a shock absorber that rests on a fulcrum placed on a connecting triangle, which is linked to a set of connecting rods (pull rods) and the swing arm. Figure 10 shows this layout.

Figure 10 Rear suspension model(see online version for colours)



In recent years, SRT has used several different linkage geometries for the rear suspension system of their bikes. All of these versions are based on the same underlying concept, but the dimensions and the properties of the spring and the damper are slightly different. The Fedem model in this study was based on the geometries of the Ilmor X³ 2007 model. The rear suspension was modelled, as shown in Figure 10, by connecting a spring (1) and a damper (2) between the parts (placed below the swing arm) and the cross beam (4), which was attached to the frame. It was important that the spring had the correct preload and spring stiffness and that the damper coefficient was correct in both compression and extension.

The primary spring (1) and the damper (2) were represented by Öhlins' TTX36 monoshock unit, which is shown in Figure 11. The free joint (3) between the link (triangle) and the cross beam at the frame had the properties of the top out spring and the end stops, which limited the maximum movement of the suspension. The reference points (4) illustrate the points of connection to the main frame. The cross beam on top of the figure had a rigid connection to the frame, whereas the swing-arm and the pull rods had revolute connections to the frame.

After all of the other bike components had the correct weight and CG, the preload of the spring in the rear suspension was adjusted to obtain the correct bike height after the bike settled on the ground. The initial equilibrium iteration in Fedem was useful for tuning the spring preload. The primary rear spring had a stiffness of 92 [N/mm] and a preload of 8 [mm]. The top out spring had a stiffness of 93 N/mm and a length of 7.5 [mm]. The static load on the rear wheel was 1033 N. The Ilmor model was assembled in

its equilibrium position (1G); therefore, the real preload plus the stroke length from the fully extended to the equilibrium position was set as the preload on the suspension springs in the model. Thus, an equilibrium preload of 27 mm on the rear spring in Fedem was obtained because the preload of the real bike is 8 mm, and the static payload compressed the spring to 19 mm. Thus, the static sag from the weight of the bike and rider compressed the rear suspension to 19 mm, as measured from the fully extended and preloaded spring. The damping in the rear suspension was created using curves of the damping force versus the damping velocity. These curves were measured by Öhlins, which supplies suspension units to most of the teams in the MotoGP series. The damper coefficients were found from calculating the derivatives of these curves with respect to the damper velocity (i.e., the curve rates). The modelled damper was the Öhlins' TTX36 monoshock unit that is shown in Figure 11.

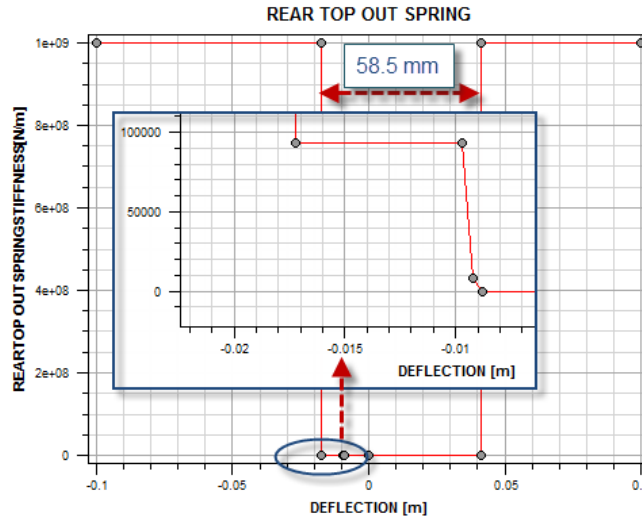
Figure 11 Öhlins TTX36 monoshock damper (see online version for colours)



To verify that the model had the correct suspension properties, the rear wheel force (vertical direction) was plotted against the measured wheel stroke. The results showed that the model results corresponded to data that was measured for the real bike. Thus, the springs in the rear suspension in the model had the correct stiffness and preload. The damper was similarly tested by measuring the damping force as function of the damping velocity, and the results were compared to curves from Öhlins. This damper test was performed by adding a vertical force to the wheel axle, and the spring stiffness was set to a value near zero (10 N/m) to enable the damper to absorb all of the force. The results showed that there was a very good correspondence between the model and the real damper. The detailed properties and tuning of the rear suspension spring and damper are described in Giussani (2007) and Weiby (2007)

The most important considerations in adjusting the shock absorber are the weight of the rider, the weight of the bike, the spring stiffness, the progression in the link and the rider's individual preferences. The maximum stroke of the rear shock was calculated from the geometry of the suspension link system, the length of the swing-arm and the given maximal wheel stroke. The rear wheel was allowed to travel 130 mm. This length equalled a shock travel of 58.5 mm. The distance between the end stops in the rear spring in the model were therefore 58.5 mm, as shown in Figure 12. When the bike and rider were stable in an equilibrium position, the suspension moved 41.2 [mm] in compression and 17.3 [mm] in tension.

Figure 12 Rear top out spring model (see online version for colours)

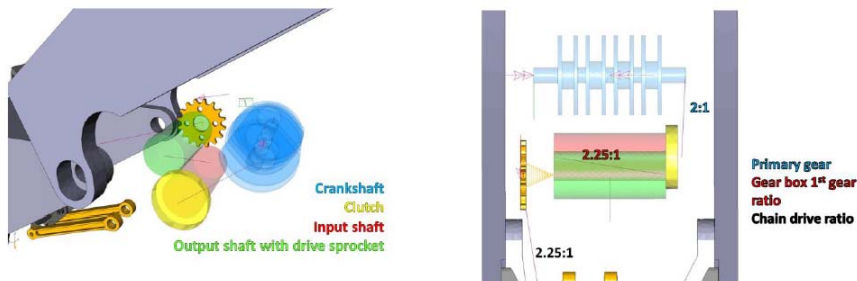


5.9 Engine and transmission modelling

The engine components were included in the model to account for the gyroscopic effects from the rotating engine and the transmission axles and to apply the same torque on the crankshaft as delivered by the real engine. No gear changes were performed during the simulation, and all of the analyses in this case were performed for a gear ratio that was equal to the first gear of the real bike. However, other gear ratios could be easily introduced into the simulations. Gear connections between the rotating parts were modelled by creating a joint that became the input shaft on one part and another joint that became the output shaft. These two joints were linked together to a gear connection, and a gear ratio was applied. This method for creating gears ensured that no back-clash or free play would occur in the modelled gear. Nonlinear joint springs could be applied to incorporate the effects of free play or back-clash.

The correct rotational speed of the engine (crankshaft) was achieved by using gear connections between the engine components and the wheel. The actual gear ratios are shown in Figure 13.

Figure 13 Ilmor X³ transmission model (see online version for colours)



These ratios could easily be changed to test other gear ratios or bike velocities. The torque delivered to the crankshaft was controlled using the curve of the real measured torque versus the engine speed. Thus, the correct torque was delivered to the rear wheel for all possible engine speeds. Later in this paper, we show that the control system in the model could regulate the torque delivered from the crankshaft to the rear wheel.

The gear ratios were based on an overall gear ratio from the crankshaft to the rear wheel of approximately 10.1:1. As previously mentioned, the primary drive ratio was set to 2:1, the front sprocket had 16 teeth, and the rear wheel sprocket had 36 teeth, corresponding to a chain drive ratio of 2.25:1. Thus, the first gear ratio in the gear box had to be approximately 2.25:1 to achieve an overall ratio of 10.1:1. The front chain sprocket was fixed to the output shaft of the gear box. Figure 13 shows these gear ratios that were implemented between the engine components and the rear wheel.

The primary rotating transmission parts were the crankshaft, the primary gear, the clutch and the input and output gearbox shafts. The characteristic properties of these components were the masses and inertias. Inertia affects bike performance because these rotating parts are connected together, producing an equivalent flywheel effect. These inertias were small relative to the inertias of the wheels; however, the rotational velocity of the driveline was much higher than that of the wheels, which significantly affected the gyroscopic properties of the bike. The locations of all of the transmission components are listed in Weiby (2007) (Appendix A). These components were located at approximately the same (CG) location as in the real bike. The weight of the rotating parts was represented by the FE models or lumped into the frame CG, and the inertia of the rotating parts was incorporated into the CG of each component to simulate the correct gyroscopic forces. The rotating inertias that were incorporated into the engine components are shown in Figure 14.

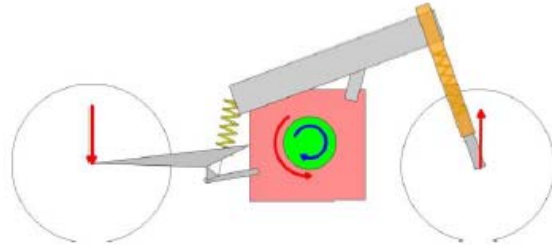
Figure 14 Transmission inertias (see online version for colours)

Component	Inertia about rotation axis
Crankshaft	0.0085 kgm ²
Clutch	0.0065 kgm ²
Input shaft	0.0055 kgm ²

The crankshaft rotated in the same direction as the wheels, thus increasing the overall gyroscopic effect of the bike. Some bikes use a counter-rotating crankshaft primarily to reduce the overall gyroscopic stability of the bike and to allow the bike to roll into corners more quickly (ImechE, 1998). A counter-rotating crankshaft can also be used to provide additional pressure on the front wheel, which allows the bike to accelerate further before a wheelie occurs. These effects have been demonstrated in Fedem Technology (2013). When a counter-rotating crank is used on real bikes, an additional gear is needed to switch the rotating direction before the gearbox. Some friction inevitably occurs in gears: the extra gear absorbs this energy. Thus, a trade-off is required between making the bike as agile as possible and delivering the maximum amount of power to the wheel.

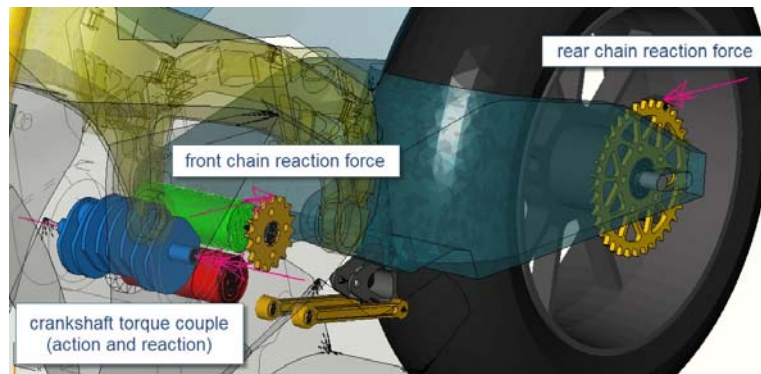
Applying a positive torque to the crankshaft turns it in the same direction as the wheels. A reaction torque must be applied to the engine housing at the same time. The direction of this reaction torque is opposite to that of the torque delivered to the crank and creates a lifting force on the front wheel. Figure 15 shows this effect.

Figure 15 Crankshaft reaction forces (see online version for colours)



In the Fedem model, these torques were applied just as explained above, i.e., a torque was applied to the crankshaft, and a reaction torque of the same magnitude but in the opposite direction was applied to the engine housing. These torques operated along the same axis that passed through the centre of the crankshaft (see the red arrows in Figures 13 and 16).

Figure 16 Applied chain reaction forces (and crankshaft torques) (see online version for colours)



5.10 Chain forces

The chain pull effect has a great impact on the rear suspension stability and the tyre grip both during acceleration and engine braking. The control system in Fedem calculated the chain force, which was based on the torque delivered to the clutch by the engine and the actual gear ratios. The modelled chain force did not cause the bike to move forward but created a secondary effect that was important to include in the model. In a real bike, the chain force creates this secondary effect, which is a compression of the rear suspension when the bike accelerates. The chain force was included in the model for this reason. To drive the bike forward, a gear joint was created to transmit the torque from the engine to the centre of the rear wheel.

The direction of the chain force was always set to be tangential to the top of the front and rear sprocket, which was the point at which the chain got into grip with the front sprocket and left the rear sprocket. This force was applied both at the front sprocket and the rear sprocket but in opposite directions, such that the opposing chain forces pointed towards each other. This force equalled the tension in the chain, which in turn led to the compression of the rear suspension. Figure 16 shows these chain forces. The rotation of the front and rear sprocket prevented the chain forces from being directly applied to these

components. This problem was solved by applying the rear chain force to a triad attached to a super-node (triad) on the swing-arm at the same location as where the chain would leave the rear sprocket. At the front, the reaction chain force was applied to the engine housing on a super-node (triad).

5.11 Clutch modelling

The purpose of the clutch is to disconnect the transmission between the crankshaft and the rear wheel. Especially at the start of the simulations, the clutch enabled the crankshaft to be accelerated without driving the entire bike. However, when the crankshaft reached a reasonable speed, the clutch could be engaged gradually and enabled the bike to start gently but quickly without losing too much engine speed.

The clutch was located on the same axis as the input shaft of the gearbox and rotated at half the speed of the crankshaft because the primary drive had a gear ratio of 2:1. This gear ratio required that the clutch transferred twice the torque delivered from the crankshaft. The maximum torque that could be transmitted through the clutch was set to twice the maximum available torque on the crankshaft when the bike accelerated. In this case, the engine drove the rear wheel, but the rear wheel often tried to drive the engine when the bike was decelerating. This behaviour is known as engine braking or engine drag. The model allowed for some engine braking because the engine allowed some negative torque on the clutch joint before the clutch joint started slipping. The maximum negative torque on the clutch in the model was set to 40 Nm, which was less than 25 % of the possible torque transmitted during acceleration (300 Nm). Real racing bikes use slipper clutches, which disengage the clutch during deceleration to reduce engine braking and provide more grip on the rear wheel and a smoother entry into and through curves.

The clutch was simulated using a spring with a maximum capacity of twice the torque delivered from the crankshaft. Exposing the clutch to a higher torque would cause the spring to yield and act as a slipping clutch. The spring stiffness was activated after 0.1 seconds, and the stiffness rose from zero to its maximal stiffness after 0.3 seconds. That is, the clutch slipped in the first 0.1 seconds and thereafter gradually made contact with the input shaft of the gearbox. The inertias of the clutch and crankshaft and their initial rotation before the clutch was engaged resulted in the clutch transmitting twice the torque delivered by the crankshaft. Thus, the clutch slipped for the first 1.5 seconds of the simulation when the maximum available torque was used. On a real bike, the clutch operates on the friction between sliding plates (i.e., the flywheel and the clutch plate). A non-linear friction clutch was tested in Fedem but did not perform well because of the high torques and velocities involved. The spring clutch system was numerically more robust than the friction-based clutch model.

5.12 Tyre modelling

An ideal racing tyre will give grip, feel and stability to a bike. These properties are in opposition to each other because grip normally comes at the expense of stability. To get grip, the largest possible contact patch should be used. Thus, the tyre should be flexible, which in turn means that the tyre will deform upon loading as stated in Pacejka (2002).

Almost all of the forces acting on the bike are transferred from the tyre/road interfaces through the suspension system to the main body. Therefore, an accurate tyre model is needed to produce the correct transfer of traction/braking and cornering forces

through the tyre. The tyres used in motorcycle racing usually have a friction coefficient above 1 and are often approximately 1.2 to 1.3 when preheated. The friction coefficient μ for the Ilmor tyres is estimated to be 1.3, as shown in Weiby (2007).

When a bike is accelerating in a straight line, the rotational deformation of the tyre is an extremely important factor that affects the possible longitudinal forces. Some deformation is necessary to minimise wheel slip. A tyre that is very stiff in the longitudinal direction cannot allow for quick changes in the longitudinal forces before critical slip occurs. Compared to car tyres, motorcycle tyres have to accommodate large camber angles without allowing for much slip.

The actual weights of the tyres were added in terms of the belt mass in the tyre model files. The front tyre weighed approximately 5 kg, and the rear tyre weighed 7 kg. This weight created the inertia of the tyres, which affected the behaviour of the tyres when they deformed. The radial stiffness of the tyres was based on calculations and measurements that SRT performed on the real tyres. The radial stiffness at zero camber angles was 0.192 kN/mm for the front tyre and 0.227 kN/mm for the rear tyre. These data were inserted into the Fedem tyre model file. The main tyre dimensions are listed in Table 1. These tyre dimensions are included in the tyre model file and can be found in LMS (2014) (Appendix J).

Table 1 Tyre dimensions

	<i>Width [mm]</i>	<i>Outer radius [mm]</i>	<i>Outer rim radius [mm]</i>
Front tyre	120	301.5	209.5
Rear tyre	200	330.7	209.5

Complete tyre models for motorbike racing tyres are highly proprietary; thus, generic magic formula (MF) tyre models were used in these simulations (Pacejka, 2002; Pacejka and Bakker, 1991). The only tyre models available are based on measurements of Michelin Pilot Road 120/70R17 and 190/50R17 tyres, which are not even made for sportive driving on public roads. Therefore, the author tried to adapt the freely available tyre model to the measured tyre properties supplied by SRT (Giussani, 2007). However, only ride simulations of wheelies and stoppies are considered in this paper, and the tyre properties in handling are not critical.

5.13 Rim modelling

The rims on the real bike are made of forged magnesium, but the exact rim geometry is unknown. The known mass and inertia were therefore lumped into the CG of the rim models. That is, the rims in the model were very stiff and had the same weight and moment of inertia as the real rims. Forged Marchesini magnesium rims with spacers and bearings weigh approximately 2.72 kg and 3.5 kg for the front and rear wheels, respectively. These forged magnesium wheels have been substituted for the cast magnesium wheels that were previously used in the MotoGP and the Superbike, resulting in a weight reduction of 1.2 kg for a set of wheels (Marchesini, 2007). The weights of the complete wheels with tyres were 9.06 kg and 10.48 kg for the front and rear wheels, respectively (Giussani, 2007). This mass reduction greatly impacted the gyroscopic effects and hence the ride and handling performance.

5.14 *Driver control modelling*

A motorbike FE assembly model is singular and unstable in most situations. Steering, balancing, breaking and acceleration commands must be implemented to control the bike in the way a driver does. These tasks are normally performed by humans based on sense impressions that are continuously and automatically evaluated by the human brain. However, in this study, the rider was modelled as rigid/static because only ride behaviour (wheelies and stoppies) was simulated. In handling simulations, the rider significantly affects bike behaviour, but SRT has confirmed that the rigid/static rider assumption is valid for sensitivity simulations of wheelies and stoppies (Giussani, 2007; Weiby, 2007).

The geometry of the front fork assembly and the gyroscopic tyre, rim and engine torques stabilise the bike as long as the bike has gained some velocity. Anyway, several other difficulties must be overcome before the Ilmor model can steer or perform a specific manoeuvre. Real bikes are driven by the best riders in the world, and some of these bikes have sophisticated electronic systems that assist the riders in controlling the extreme forces exerted on these bikes. Developing a control system that can perform the same manoeuvres as smoothly and quickly as these riders do is obviously a major challenge.

In addition to the steering system that enables the bike to manoeuvre and maintains its balance, a control system is needed to calculate the engine performance. The dependence of the engine torque on the engine speed is a primary engine characteristic. The system must include a clutch, and the system behaviour must be controlled. The chain forces have important effects on the overall behaviour of a motorbike, depend on the actual torque from the engine, and must be calculated in real time by the control system. The control system should also define the target velocity and how much of the available torque should be used to achieve this speed. The control system also calculates the speed-dependent air drag that acts on the bike.

The overall control system was constructed from a set of mathematical control blocks. The input and output blocks connected the control system and the mechanical FEM assembly model. The control blocks were used between the input- and output-blocks and consisted of amplifiers, binary-input blocks, integrator blocks, non-continuous blocks and PID controllers (PI, PD and PID).

5.15 *Steering control*

The Ilmor control system model included a section that calculated the steering signals. This steering system consisted of two parts. The first part maintained the balance of the bike and ensured that the bike did not capsize. The second part could create a set of steering commandoes that make the bike manoeuvrable and able to ride curves. These steering signals enabled the control system to act almost like a real driver is steering the bike.

To limit the maximum turning angle of the front fork and the front wheel, a spring was added to the revolute joint that enabled the fork to rotate around the steering stem axis. This spring had no effect before the turning angle reaches ± 20 degrees but became extremely stiff beyond this angle. This revolute spring restricted the steering angle to the real bike steering limits.

A light damper (10 Nms/rad) was applied to the revolute joint that was attached to the steering stem axis to reduce vibrations in the steering (and the rest of the bike) from short steering pulses that were created by the control system. No friction was included in the revolute joints around the steering stem axis; therefore, only the inertia of the fork and its components provided a delay in the turning movement of the fork without the steering damper. The control system regulated the magnitude and the sign of the torque applied to the steering column. Without the inclusion of the steering damper, this torque caused the front wheel to vibrate because of the absence of friction in the bearings. The damper helped to stabilise the fork assembly relative to the frame and ensured that the entire bike moved more smoothly.

The stability of the bike was controlled by measuring the roll angle of the frame (at two reference points) and by applying torques to the triple clamp at the steering stem axis to minimise the roll angle. That is, the measured angle of the frame was used as input data to the steering system. The magnitude of the applied steering torque depended on the size of the roll angle. When the bike leans to the left, the control system should create an output torque to the steering that turns the front wheel to the left. Thus, the front wheel rides in under its CG, and the bike returns to a balanced state. The value of the roll angle (which was calculated at the two reference points) was hence used as an input to a PID-regulator, which changed the applied torque that controlled the front wheel. To avoid severe vibrations and abnormal riding, a torque limiter was applied after the PID-regulator (± 300 N). A normal rider could not apply a larger steering torque.

With its front wheel in the air and the steering turned to the left, the bike will lean to the right. This gyroscopic effect is well known among skilled stunt riders, who use it to maintain balance when performing wheelies. Thus, the height of the front wheel axle was measured to enable the control system to make a switch. If the height was larger than the free radius of the tyre, the steering torque was multiplied by zero; otherwise, the steering torque was multiplied by one. Thus, the steering system was only active when the front wheel had ground contact. The tyre deflection under loading resulted in the tyre radius normally being less than the free tyre radius. A height-measuring switch was also added to the rear wheel, which turned off the steering torque if the rear wheel did not make contact with the ground.

The counter-steering method has been shown to be the most effective method for steering a motorbike but is challenging to implement in a simulation model. For example, to turn the bike to the left, the control system steering the bike should initially turn the steering to the right to roll the bike to the left. The next operation should be to steer the bike into the turn by turning the bike to the left. A simple turn actually requires at least two steering signals in opposite directions.

When a steering torque is applied to the fork assembly at the centre of the headstock, a reaction torque must also be applied to the frame (by Newton's third law). This reaction torque must be of the same magnitude as the steering torque and act along the same axis but in the opposite direction. The torques applied at the top of the headstock (number 1 and 2) were the balancing steering torque and its reaction torque, respectively. The torque pair at the bottom of the headstock (number 3 and 4) were the steering command and its reaction torque, respectively (see Figure 18). The torques corresponded to the steering and frame reaction forces that would be applied to the handlebars by the rider in a real situation. The complete steering control system is shown in Figure 17.

Figure 17 Steering control system

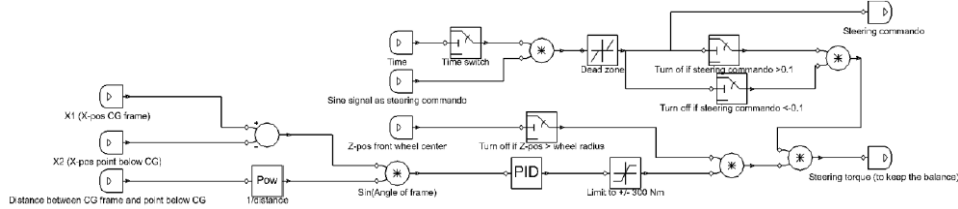
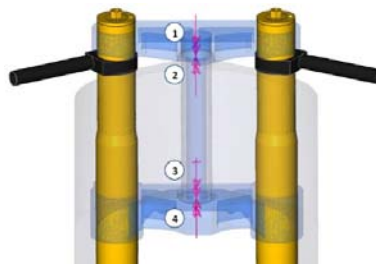


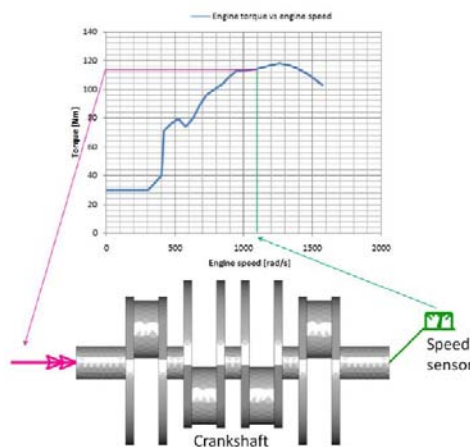
Figure 18 Applied steering torques (see online version for colours)



5.16 Engine control

The engine performance was also modelled by a control system. The specified engine torque (as a function of engine speed) was used as an input function to the control system. The engine characteristics were based on measurements from the real bike. Figure 19 shows the underlying concept of engine torque control. The system constantly measured the speed of the crankshaft and applied the maximum available torque at this speed, which in turn resulted in a change in the crankshaft speed. The system operated in a constant loop until the maximum crankshaft speed was reached (approx. 2,000 [rad/sec] / 19,100 rpm).

Figure 19 Engine control (see online version for colours)



The real engine does not deliver an output torque below 2,865 rpm. An initial torque of 30 Nm was therefore applied below this limit to jump start the simulation. This initial torque ensured that the engine always produced a forward rotational movement. The engine control system also allows the user to control how much of the available torque the engine delivers over a given bike speed interval.

When full throttle is applied to the lower gears, the bike lifts the front wheel very quickly because of the available torque [wheelie]. To produce the best possible acceleration times with the model, a torque limiter that reduces the engine torque if the front wheel lifts was included in the engine control system. The engine control system also included blocks to determine the engine torque that should be delivered for specific bike or engine speed ranges. These blocks may act as rpm-limiters on real bikes or as speed limiters, such as those used when MotoGP bikes ride in the pit-lane.

5.17 Chain force control

The chain force was calculated from the engine torque and the gear ratios (crankshaft vs. rear wheel). The control system that calculated the chain force also calculated the clutch contact ratio. That is, the chain force was reduced when the clutch skidded. The front and rear sprocket exert chain forces were parallel but acted in opposite directions (see Figure 16).

Thus, the chain forces were in equilibrium and did not cause any translation of the entire bike (i.e., the bike was at equilibrium). However, the chain forces affected the movement of the swing-arm relative to the chassis. This movement affected the compression or extension of the rear suspension. The chain force control system is illustrated in Figure 20.

Figure 20 Chain force calculation

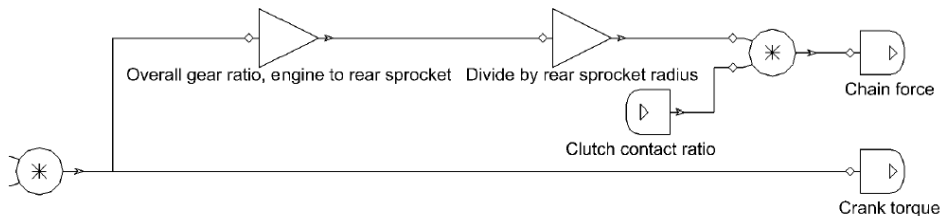


Figure 21 Adjustable wheelbases (see online version for colours)

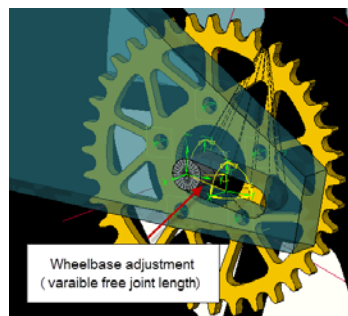
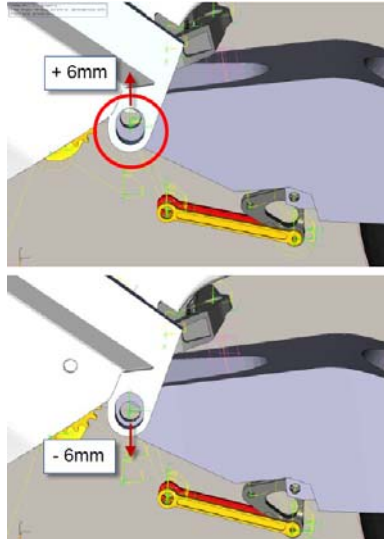


Figure 22 Adjustable pivot axes (see online version for colours)

5.18 Air drag

The aerodynamic drag force is the most important factor affecting the behaviour of the bike. A lifting force from air flow also acts on the bike. This effect was not included in the simulation model. The aerodynamic drag force was calculated using the following equation:

$$F_{AD} = \frac{\rho_o \cdot V^2 \cdot C_X \cdot A}{2}$$

where

ρ_o denotes the density of air at 20 deg./1 atmosphere pressure (1.2 [kg/m³])

V denotes the bike velocity in [m/s]

C_X denotes the drag coefficient

A denotes the frontal area of the bike.

SRT provided a drag coefficient multiplied by the frontal area A of the Ilmor X³ bike of 0.27 m² (Giussani, 2007).

The aerodynamic drag force at each time step in the simulation was calculated by the control system. This drag force was applied at the front of the bike and was always opposite to the direction of travel. The control system measured the velocity of the frame CG, and the aerodynamic drag force was calculated using the formula given above.

6 Dynamic simulation of different configurations

The primary purpose of this study was to test different settings virtually for multiple manoeuvres and at different speeds to evaluate and optimise bike handling. The different test categories are given below.

- acceleration tests with different wheelbases
- testing the effect of the rotational direction of the crankshafts on bike behaviour
- testing the bike performance for different gyroscopic effects
- testing the effect of changing the position of the rear axle and the pivot axle
- testing the effects of varying the characteristics of the primary spring and the damper
- brake tests (including modal analysis).

6.1 Suspension configuration

The characteristics of the springs and the damper were varied, and the effects were tested for manoeuvres such as those previously described in this paper. Three different settings based on real measurements were implemented as rear damper property functions. One of these settings was equivalent to the default damper on the real bike, and the other two settings were alternative settings with higher and lower damper coefficients. Other damper properties could be tested by varying the property functions. In this study, suspension testing was performed to correlate the Ilmor simulation model with the real bike. The test results can be found in Weiby (2007).

6.2 Acceleration tests with different wheelbases

To test the effect of the bike wheelbase during acceleration, the results from several configurations were simulated and compared to each other. The test was to ride the bike from 0 to 100 [km/h] in the shortest possible time. The torque from the engine was automatically reduced if the front wheel lifts more than a pre-defined height above the road. This 'throttle-reduction' was equivalent to a rider's action if a wheelie occurs. Each bike configuration was identical except for the wheelbase, which was changed for each run. In these tests, the wheelbase was varied by moving the rear wheel axle forward or backward relative to the swing-arm just as is done for real bikes when the chain tension is altered. When the wheelbase was changed, the load on the rear suspension also changed because of a longer or shorter arm from the rear suspension unit to the rear wheel axle. To provide the bikes with different wheelbases, the same ride height for the preload in the rear main spring was altered in each case to match the default ride height. The original wheelbase of the model was 1,459 mm. The maximum wheelbase was 1,478.2 mm, and the shortest tested wheelbase was 1,431.3 mm.

Table 2 Results from acceleration tests with different wheelbases

<i>Bike configuration</i>	<i>Acceleration when front wheel lifts</i>	<i>Time</i>	<i>Time 0–100 km/h</i>
Long wheelbase (1,478.2 mm)	10.66 m/s ²	2.55 sec	2.97 sec
Short wheelbase (1,431.3 mm)	9.86 m/s ²	1.99 sec	3.36 sec
Original configuration (1,459 mm)	10.04 m/s ²	2.15 sec	3.09 sec

As expected, the results showed that the longest bike produced the best acceleration performance. The front wheel on this bike lifted after 2.55 seconds for a bike acceleration of 10.66 [m/s²]. The bike with the shortest wheelbase achieved the lowest accelerations before the front wheel lifted. The front wheel lost contact with the ground after 1.99 seconds for a bike acceleration of 9.86 [m/s²].

It is well known among bike designers and riders that a bike with a long wheelbase is more stable when riding straight forward than a shorter bike and that the long bike is also harder to turn. This behaviour results from the increase in the inertia and gyroscopic effects of the bikes upon increasing the wheelbase. Thus, a compromise must be made in track-bike design because straight line stability and acceleration are desired together with an agile steering response.

6.3 Acceleration and wheelie tests with a counter-rotating crankshaft

The reaction torque from the crankshaft to the engine housing affects the bike handling and agility. This torque acts to rotate the engine housing and the entire bike in the direction opposite to that of the crankshaft rotation. The resulting effect is that a forward rotating crankshaft (where the rotation is in the same direction as the wheels) will increase the front lifting force of the bike during acceleration. This effect is illustrated in Weiby (2007). A counter-rotating crankshaft will produce the opposite effect and exert additional pressure on the front wheel during acceleration, producing greater acceleration before a wheelie occurs. This action also improves the grip on the front tyre when the bike accelerates out of corners. This effect may be important if the initial configuration creates insufficient front weight. A comparative test was performed between the original model and an identical model in which the crankshaft was turned in the opposite direction. These models were run in an acceleration test to compare the acceleration and the front wheel loads.

Table 3 Results from acceleration tests of bikes with different crankshaft rotation directions

<i>Bike configuration</i>	<i>Acceleration when front wheel lifts</i>	<i>Travelled distance when front wheel lifts</i>	<i>Load on front wheel after 0.1 sec</i>
Original configuration	10.04 m/s ²	13.41 m	1,099.8 N
Bike with backward rotating crankshaft	10.17 m/s ²	13.69 m	1,173.5 N

Just after the start of the simulation when the engine was revving up before the clutch is released, the engine torque created either a lifting or a downward force on the front wheel depending on the rotational direction of the crank. After 0.1 seconds, the engine revved up to approximately 3,900 rpm, and the torque was 69 Nm. In the model with a

counter-rotating crankshaft, the load on the front wheel at this time was 1,173.5 N. In the original model, the load at this time was 1,099.8 N. The difference in the loads was approximately 7 kg. The results also showed that the front wheel of the bike with the counter-rotating crankshaft lifted after 13.69 m, and the front wheel of the bike with the forward rotating crankshaft lifted after 13.41 m during maximal acceleration. This lift was small and was caused by a local peak in the torque curve.

6.4 Comparative tests of gyroscopic effects on handling

Several tests were performed to test the influence of gyroscopic effects on bike performance. The first test was a comparative test of the original model against two other bike configurations, which had 50% and 75% of the original wheel inertias and gyroscopic effects. The tests were conducted with no active steering. The control system only maintained the bike in balance with assistance from self-steering from the front trail and the gyro effects from the wheels and the engine. A bike with a counter-rotating crankshaft has a smaller overall gyroscopic effect than a bike with a forward rotating crankshaft. That is, a bike with a counter-rotating crankshaft can 'fall' into a corner more easily and is more responsive to a steering commando than the original bike with a forward rotating crankshaft. The simulation results demonstrated this effect.

Four tests were conducted with different bike configurations to investigate accelerations up to 50 km/h before a steering commando was performed. A steering commando is a torque that can be described by a parabolic curve with a maximum value of 15 Nm that lasts for 0.5 seconds. Thus, the bikes were exposed to the same force from the steering, which resulted in a bike roll angle that depended on the gyroscopic moment of the bike. The maximum roll angle was measured after a specific time in all of the simulations. Two similar tests were performed to determine how changing the speed of the steering torque affected the bike behaviour. First, the bike speed was increased to 80 km/h, and the same steering commando was applied; finally, the steering torque was also increased to a maximum value of 35 Nm.

The test results are given in Table 4 showing that the inertia (and weight) of the wheels had a major impact on the overall behaviour of the bikes. Using a backward rotating crankshaft had a rather small effect, but the results showed that this bike was slightly more responsive to a steering signal than the original bike. The percentage difference in the roll angle between the original bike and the bike with a backward rotating crankshaft increased at higher velocities. This increase depended on the engine revs and the choice of riding gear. Riding at a high speed in a high gear produced a low engine speed, i.e., the gyroscopic effect from the crankshaft was small compared to that from the wheels. These tests were performed in first gear.

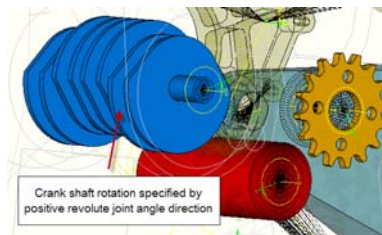
Additional tests were performed to test the stability of two different bikes. The original bike and a bike with wheels with 50% of the inertia of the wheels of the original bike were accelerated to 100 km/h (in 3.2 seconds) before the bikes settled down to a constant speed. The steering systems were not activated in these tests. The original bike was able to ride steadily and did not drift very far away from the initial straight line. The bike with wheels with 50% of the gyroscopic effect from the wheels of the original bike was more unstable: larger roll angles were obtained than those for the original bike, and the bike also drifted more obviously away from the initial line.

Table 4 Results from handling tests of bikes with different crankshaft rotation directions

<i>Bike setup</i>	<i>Frame angle after 15 Nm steering commando at 50 km/h</i>	<i>Frame angle after 15 Nm steering commando at 80 km/h</i>	<i>Frame angle after 35 Nm steering commando at 50 km/h</i>	<i>Frame angle after 35 Nm steering commando at 80 km/h</i>
Original bike	20.49°	10.95°	31.62°	27.77°
Bike with 50% inertia wheels	90° (tip over)	90° (tip over)	90° (tip over)	90° (tip over)
Bike with 75% inertia wheels	25.75°	14.32°	90° (tip over)	90° (tip over)
Bike with backward rotating crankshaft	20.98°	11.44°	32.79°	31.14°

6.5 Comparative tests for different pivot axis locations

The pivot axle, which connects the swing-arm to the main frame, is movable in the vertical direction. Figure 23 illustrates the two different settings of the pivot axle position that were tested in Fedem. The axle is moveable on real bikes primarily to alter the effect of the chain forces. The chain forces have both positive and negative effects on the suspension performance and hence the behaviour of the entire bike. The positive effect is that the chain tension stabilises the rear suspension by compressing the spring and the damper during the acceleration of the bike. The chain pull tends to lift the swing-arm, whereas the driving force that is transmitted to the ground pushes the wheel axle forward. The pivot axle is positioned higher than the rear wheel axle; therefore, the driving force lifts the frame relative to the swing-arm and creates more traction by pushing the wheel against the ground. The forward traction raises the frame to a height that, among other factors, depends on the force delivered and the position of the pivot axle. The lift of the frame in the rear and the increasing angle of the swing-arm can be observed for real bikes in acceleration, and it is especially easy to observe when a dyno-test is run on a bike to measure its engine power. When the throttle is released and engine braking starts, the rear wheel tries to drive the engine, and the chain tries to push the rear tyre off the ground. That is, the action of the chain produces negative effects during engine braking but positive effects during acceleration. For the bike to ride fast and maintain its grip, a smooth deceleration is necessary as the throttle is released, and no jerks that would cause the swing-arm to move should occur. These negative effects from the action of the chain during braking are why slipper-clutches are used on racing bikes.

Figure 23 Crank shaft rotations (see online version for colours)

When the pivot axle is moved the length of the rear spring, the damper must also be changed to ensure that the suspension has the same characteristics as that of the original bike. In the following test, the initial wheelbase was kept unchanged. The length of the spring and the damper were automatically corrected in Fedem when the link to which the suspension unit was connected moved. Thus, the spring stiffness, the preload and the damper properties in the tests were equal to the settings of the original bike. When the pivot axle moved 6 mm down, the length of the spring in the model was approximately 0.282 m, and when the pivot axle moved 6 mm up, the spring length was approximately 0.278 m. In the test that was performed, the maximum acceleration ranged from 0 to 100 km/h before the velocity became constant at 100 km/h. The control system reduced the engine torque when a wheelie occurred in each test, just as a real rider would do. In these tests, the maximum allowed height of the front wheel axle was set to 0.4 m, which equalled a distance of 9.95 cm from the ground to the tyre. After each test was performed, the time and the acceleration of the bike when the front wheel lost contact with the ground was sampled and are listed in Table 5.

Table 5 Results from tests with different pivot axle heights

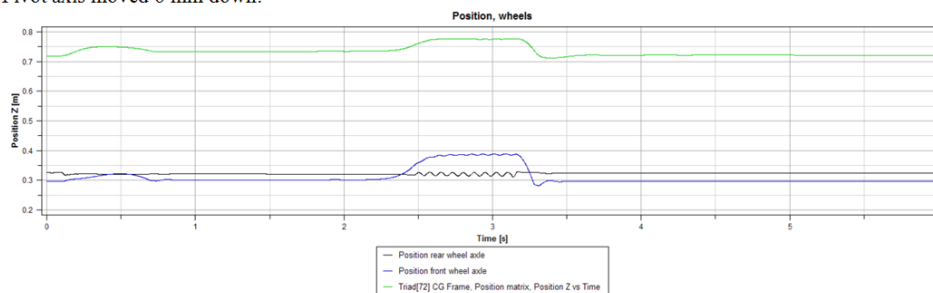
<i>Bike setup</i>	<i>Acceleration when front lifts</i>	<i>At time</i>
Pivot 6 mm up	10.11 m/s ²	2.19 sec
Pivot 6 mm down	9.89 m/s ²	2.13 sec
Original	10.04 m/s ²	2.15 sec

Figure 24 Wheelie tests with different pivot axis locations (see online version for colours)

Pivot axis moved 6 mm up:



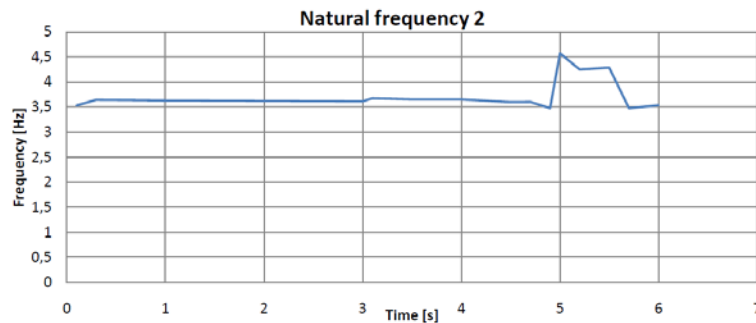
Pivot axis moved 6 mm down:



The bike with the highest pivot position allowed the highest acceleration before a wheelie occurs. The reason for this result was investigated by repeating the tests without applying chain forces. Very similar behaviour to the previous test was observed. The effects of the

chain force in the model changed when the pivot axle was moved. When the axle was moved upwards, the compression of the rear suspension during acceleration was reduced because of the shorter torque arm from the chain force to the pivot axle. Thus, the front wheel lift decreased when the pivot axle was moved upwards. The tendency of the frame to lift at the rear during acceleration increases when the pivot axle is moved upwards, which was confirmed in the simulations. When bikes with different pivot axle positions ride at constant speed, they have the same frame heights; however, during acceleration, the bike with highest pivot position obtains the greatest frame lift. This result is illustrated in Figure 24, which shows measurements of the vertical position of the frame and the front and the rear wheel axle. The first 3.2 seconds of the test involved acceleration with a small wheelie. After 3.2 seconds, the bikes maintained a constant speed.

Figure 25 Variation in natural frequency (mode 2) from non-linear effects (see online version for colours)



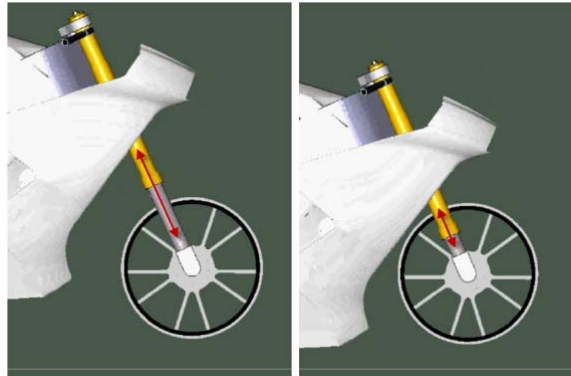
6.6 Modal analysis

Previous advances in modelling motorcycle dynamics improved the understanding of the principal flexible modes during straight-running and steady state cornering conditions. These earlier studies showed that under certain operating conditions, some of the vehicle modes can be lightly damped or even become unstable. The most important race bike modes are wobble, weave and pitch. Wobble is a steering oscillation that is similar to the caster shimmy that can occur for the front wheels of supermarket carts, whereas weave is a fishtailing-type motion involving roll and yaw (Evangelou et al., 2006). The FE-based model was used to study the vibration modes of a motorbike during a specific test procedure in which the bike was not at steady-state. Mode shape analysis was performed at selected time steps during a dynamic Fedem simulation. Non-linear effects from large deflections and stress stiffening (during braking operations) were incorporated into the simulation. As an example, the ten first natural frequencies of the bike were sampled during a simulation in which the bike accelerated to and maintained a constant speed for a short period before decelerating and stopping after 6 seconds.

The simulation involved light braking after 4.5 seconds and increased to maximum braking after 5 seconds. The braking compressed the non-linear front springs and increased the stresses in the fork legs. The braking increased the natural frequency of mode number 2, which was related to the fork suspension unit. The frequency was

initially 3.53 Hz and increased to a maximum of 4.51 Hz because of the spring compression and stress stiffening during braking. The shape of mode number 2 is illustrated in Figure 26.

Figure 26 Fork compression mode shape (see online version for colours)



7 Discussion

The Fedem Ilmor modelling and correlation has produced a virtual prototype that includes many of the dynamical properties and effects of the real motorbike during racing. However, a simulation model is always a trade-off between efficiency and accuracy, and not all effects could be included. In this section, some of the effects and limitations of the model are discussed.

This model is not an exact geometric representation of the real Ilmor bike because many of the bike parameters were not available. The stiffness, weight and CG of some of the components were unknown and were approximated to produce the correct overall mass and stiffness distribution of the Ilmor bike. These simplifications may have introduced errors into the dynamical properties, but the inertia of the rotating parts and hence the gyro effects were accurate.

The tyre models in this simulation were based on modified car tyres and did not incorporate the correct cross-sectional shape of real motorcycle tyres. This simplification introduced limitations for handling simulations. However, the tyre models performed well in the ride simulations, and acceleration and braking results were obtained that corresponded well with the real tests and SRT observations. The real Ilmor motorbike has rubber bushings in its suspension units to reduce stresses and vibrations and seal parts that contain oil or liquids. Although such rubber bushings could be modelled in Fedem, some minor rubber components were neglected because their properties and computational time were not available.

The ride and handling tasks that are normally performed by human riders were performed by a digital control system in the dynamic simulations. The feeling and response that human beings can provide when riding a motorbike are essential for fast and safe MotoGP performance. It is not easy to replace an experienced driver with a control system. The author obtained a motorcycle driving license to experience and become familiar with the characteristics of a race bike.

There are several sources of vibrations in a motorcycle. Vibrations may be produced by the engine from ignition, and other vibrations may result from the necessary slack in the chain that results in a swinging movement of the chain during riding. Several other sources also affect the behaviour of the bike. These vibration sources were too complex to be included in the Fedem model.

8 Summary

This study has shown that certain characteristics of a MotoGP bike can be modelled, simulated and optimised. A simplified but reliable model of a racing bike was created using the finite element method. The meshed parts were assembled into a functional assembly FEM in Fedem. The individual FE models were connected by springs and dampers and revolute, ball and free joints. Forces, tyres and a control system were implemented to make the model function as a motorcycle handled by a human driver. The model could be reconfigured for a different mass and stiffness distribution. The lumped springs and dampers could be modelled using non-linear functions based on physical tests. The mechanical topology and control system could easily be modified to change the applied forces and torques or the resulting inertia and gyro effects. Different bike settings were tested, and the effects of these changes were studied.

The simulation results showed the effects of different bike configurations and demonstrated that the virtual motorbike is realistic and potentially useful. Most of the tests were focused on improving the acceleration performance and avoiding the wheelie effect. The best acceleration performance was obtained using a long wheelbase, an elevated pivot axle (which connected the swing-arm to the frame) and a backward rotating crankshaft. This configuration also exhibited several drawbacks that were related to the handling performance of curves, and reduced power was delivered to the wheel because of the reversed crankshaft. The acceleration times that were obtained corresponded well with the performance of the real Ilmor MotoGP bike. The simulations showed that the default configuration of the Ilmor bike could accelerate from 0 to 100 km/h in approximately 3 seconds without wheelies.

The influence of gyroscopic effects on ride and handling were confirmed by the simulations. A bike with low inertia wheels, and thus low gyroscopic forces, was more unstable but also more responsive to steering signals than a bike with higher inertia wheels. These results should be considered to be sensitivity results because tyre models with accurate handling properties were not available.

In this paper, we showed that a dynamic simulation in Fedem (Pacejka, 2002) can produce realistic results even using a simplified bike model. Most of the dynamic race bike behaviour could be simulated, but considerable information on the geometry, the material properties, the engine data and suspension properties are needed. Further mass and stiffness optimisation based on modal analysis could be performed as well as a detailed fatigue analysis. A FE-based simulation model could therefore serve as an effective tool in race bike development. The modelling and simulations tasks are challenging but provide results that would be more time consuming and difficult to measure and observe using physical prototype testing. The model was used to illustrate how flexible vibration modes are affected by non-linear springs and structural stress stiffening during hard braking operations.

9 Further work

Different configurations should be modelled and tested before building a real bike. This approach is used to obtain advance information and design improvements at minor prototype costs. The simulation model can be used to determine the parameters that most affect the desired performance (i.e., to perform a sensitivity study). If the exact geometries of the components are available, the stiffness and stress distributions can be tested and optimised using the same simulation model.

The modelled suspension systems are fully adjustable, and it would be interesting to study other suspension settings. The ride height could also be adjusted to move the CG of the bike, thereby simulating other handling properties.

The movements of the human rider could also be taken into account. Usually, the rider leans forward when accelerating, thus reducing the wheelie effect compared to when the rider behaves as a fixed mass in a 'neutral position'. A simplified simulation model of a bike where the rider is modelled as a fixed mass could indeed be used in further studies of motorcycle simulations, but the rider can have a critical effect on the bike in some situations.

Further refining the clutch and the control system will improve the acceleration performance of the bike. The current Ilmor model does not handle very high initial engine revs because of limitations of the clutch model. Thus, some time elapses before the model reaches the optimum engine speed where the maximum torque is available.

Achieving reasonable behaviour of the tyre models was a major challenge in this study. When the bike model rode in a straight line (without a large camber angle), the behaviour of the bike and the tyres were realistic. The existing tyre model did not perform realistically in cornering, and a better tyre model that can accommodate large camber angles should be implemented. Additional funding for tyre testing and parameter identification is needed to obtain a reliable tyre model.

Acknowledgements

The author wishes to thank SRT for providing him with a challenging project and access to model inputs and component test results. The project inspired the author to become a biker: he found that physical testing was more fun than he thought it would be!

References

- Cheney Engineering (2007) *Fork Clamps, for Head Adjusters, Handle Bar Mounts & More ...* [online] <http://www.flattrackaccessories.com/forkclamps.shtml> (accessed 7 June 2007).
- Cossalter, V. and Lot, R. (2002) 'A motorcycle multi-body model for real time simulations based on the natural coordinates approach', *Vehicle System Dynamics*, Vol. 37, No. 6, pp.423–447.
- Crash Media Group (2006) *Ilmor X³ Ready for MotoGP Race Debut* [online] <http://www.crash.net/motogp/news/78172/1/ilmor-x3-ready-for-motogp-race-debut.html> (accessed 3 December 2011).
- Evangelou, S., Limebeer, D.J., Sharp, R.S. and Smith, M.C. (2006) 'Control of motorcycle steering instabilities', *IEEE Control Systems*, Vol. 26, No. 5, pp.78–88.
- Fedem Technology (2013) *Fedem Mechanical* [online] <http://www.fedem.com/software/fedem-mechanical/> (accessed 10 February 2014).

- Frezza, R. and Beghi, A. (2003) 'Simulating a motorcycle driver', in Kang, W. et al. (Eds.): *New Trends in Nonlinear Dynamics and Control and Their Applications*, pp.175–186, Springer-Verlag, New York.
- Giussani, A. (2007) 'Statements and chassis geometry calculations [Excel Worksheet]', File: 007_chassis_calculation_vers_0107.xls.
- Hauser, J. and Saccon, A. (2006) 'Motorcycle modeling for high-performance maneuvering', *IEEE Control Systems*, Vol. 26, No. 5, pp.89–105.
- Institution of Mechanical Engineers (IMEchE) (1998) 'Automobile division', *International Conference on Multi-Body Dynamics: New Techniques and Applications*, 10–11 December, IMechE HQ, Professional Engineering Publishing, London, Bury St. Edmunds, UK.
- LMS (2014) *SAMCEF Mecano* [online]
<http://www.lmsintl.com/?sitenavid=8435E5BB-C04D-49AB-B72A-9CB01D6FD9DB>
 (accessed 23 April 2014).
- Marchesini (2007) *Forged Magnesium* [online]
<http://www.marchesiniwheels.com/ENG/Upgrade/Forged+Magnesium.htm> (accessed 12 February 2007).
- Pacejka, H.B. (2002) *Tyre and Vehicle Dynamics*, Butterworth Heinemann, Oxford.
- Pacejka, H.B. and Bakker, E. (1991) 'The magic formula tyre model', *Vehicle System Dynamics*, Vol. 21, No. S1, pp.1–18.
- Sharp, R.S. and Limebeer, D.J.N. (2001) 'A motorcycle model for stability and control analysis', *Multibody System Dynamics*, Vol. 6, No. 2, pp.123–142.
- Sharp, R.S., Evangelou, S. and Limebeer, D.J.N. (2004) 'Advances in the modelling of motorcycle dynamics', *Multibody System Dynamics*, Vol. 12, No. 3, pp.251–283.
- Sivertsen, O.I. (2001) *Virtual Testing of Mechanical Systems*, Swets & Zeitlinger, Lisse.
- Spalding, N. (2010) *MotoGP Technology*, 2nd ed., Haynes Publishing, Sparkford, Yeovil, Somerset [online]
http://www.haynes.co.uk/Press/Releases_HTML/100415_MotoGPTechPR_haynes_press_release.htm.
- Weiby, A. (2007) *Modeling and Simulation of Racing Bike*, Unpublished Master's thesis, Norwegian University of Science and Technology – NTNU, Trondheim, Norway.